Materials International
Open-Access Journal (ISSN: 2668-5728)

Article
Volume 8, Issue 1, 2026, 6
https://doi.org/10.33263/Materials81.006

Synthesis and Characterization of Zinc Oxide Thin Films for Photovoltaic Applications

Surajudeen Otolowo Azeez [1,*], Kamaldeen Olasunkanmi Suleman [2,*], Akeem Adekunle Adewale [1], Khadijat Kuburat Babalola [1], Aishat Abass Ojuolape [4], Yekinni Kolawole Sanusi [3]

[1] Department of Physical and Chemical Sciences, Federal University of Health Sciences, Ila- Orangun, Nigeria; surajudeen.azeez@fuhsi.edu.ng (S.O.A.); khadijat.babalola@fuhsi.edu.ng (K.K.B.);
[2] Department of Physics, School of Basic Sciences, Nigeria Maritime University Okerenkoko, Delta State, Nigeria; kamaldeen.suleman@nmu.edu.ng (K.O.S);
[3] Department of Pure and Applied Physics, Ladoke Akintola University of Technology, Ogbomoso, Nigeria; aaadewale38@lautech.edu.ng (A.A.A.); yksanusi@lautech.edu.ng (Y.K.S.);
[4] Department of Physics, Colorado State University, Colorado, USA; aishat.ojuolape@colostate.edu;
* Correspondence: kamaldeen.suleman@nmu.edu.ng (K.O.S.); aaadewale38@lautech.edu.ng (A.A.A.);

Received: 28.05.2025; Accepted: 7.07.2025; Published: 10.03.2026

Abstract: Owing to its potential to significantly improve photovoltaic performances of solar cells, zinc oxide nanoparticles (ZnO NPs) thin films have attracted significant interest from researchers working towards enhancing the performance of organic solar cells. In the present study, ZnO NPs thin films were synthesized by spin coating. The structural and morphological properties of the ZnO NPs thin films were characterized using various techniques, including X-ray diffraction (XRD), scanning electron microscopy (SEM), and UV-visible spectroscopy. XRD analysis revealed the crystalline structure of the ZnO NPs thin films, while SEM images showed a surface morphology with a particle size distribution of approximately 36 nm. Analyses showed that the ZnO NPs thin films exhibited excellent crystallinity, uniform surface morphology, and a direct bandgap energy of approximately 3.30 eV. The photovoltaic performance of organic solar cells with a thin ZnO NPs film was tested, and the results showed a significant improvement in short-circuit current density (Jsc) and power conversion efficiency (PCE) compared to chemically prepared ZnO NPs. Investigations are underway on ZnO thin films with meticulously controlled micro-scale morphology, which are considered promising alternatives to indium tin oxide (ITO) films for various photovoltaic applications.

Keywords: TCOs; thin films; solar cells; photovoltaic; short circuit current.

1. Introduction

Recent studies have highlighted a significant increase in global electricity demand, driven by factors such as economic growth, the electrification of transportation, and the expansion of energy-intensive industries such as data centers, the paper industry, the cement industry, and the basic metal industry [1-2]. This surge in demand has raised concerns about the reliance on traditional, non-renewable energy sources, which are limited, have negative environmental impacts, and are becoming increasingly expensive [3,4]. In light of these challenges, researchers and policymakers are actively investigating alternative solutions, with a particular focus on clean energy sources. Solar energy has emerged as the most promising

renewable energy resource, capable of meeting a substantial portion of the growing electricity demand [5-7].

Transparent Conducting Oxides (TCOs) are of great importance in the fabrication of solar cells and devices. TCO thin films have attracted substantial research interest in recent years due to their widespread use in various optoelectronic devices, such as touchscreens, liquid crystal displays, solar cells, and light-emitting diodes [8,9]. Materials for use as TCOs are required to exhibit both high electrical conductivity and high optical transparency in the visible region. Indium tin oxide (ITO) is the most commonly used TCO due to its excellent transparency to visible light and high electrical conductivity [10,11]. However, one of the major drawbacks of ITO is its high cost, the insufficiency of indium, its principal constituent element [12,13], and its toxicity. Additionally, the optical and electrical properties of ITO can degrade when exposed to a hydrogen plasma environment [14-16]. As a result, there is a growing concern to find appropriate alternatives that will eradicate these shortcomings without compromising efficiency.

Recently, doped ZnO thin films with Ga, In, and Al, for TCO, have been thoroughly investigated to replace ITO thin films for applications in optoelectronics devices, including solar cells. Zinc oxide (ZnO) is a remarkable semiconductor material that has garnered considerable interest across various industries because of its distinct properties and wide range of applications. Unlike traditional semiconductor materials, ZnO offers a unique combination of characteristics that make it a highly desirable choice in the realm of solar cells [17-20], optoelectronics [21-23], sensor and biomedical [24-26] applications, and has been suggested as appropriate for use in optical waveguides [27,28]

In the present study, we synthesized and characterized ZnO thin films using the spin-coating technique. This method was chosen for its numerous benefits, including operation at low temperatures, straightforward coating of extensive areas, and suitability for creating porous films and uniform multi-component oxide films. These ZnO thin films with controlled microscale morphology are investigated as potential replacements for ITO in various photovoltaic applications.

2. Materials and Methods

2.1. Materials.

Matricaria chamomilla L. plants (chamomile flower) were collected around the campus of the Federal University Health Sciences, Ila-Orangun (FUHSI), Osun State, Nigeria. Zinc acetate dihydrate (99 % purity) was purchased from Malaysia and was used without further purification. Before the experimental procedure, all glassware and apparatus were washed with a freshly prepared Piranha etch, followed by distilled water of 18.2 MΩ.cm resistivity, after which they were dried in the oven. For the collection of the extract, Whatman filter paper Grade I was used. Distilled water was used for the entire duration of the experiment to avoid any contamination from Impurities. The extract was then stored in a sterile container at -20 °C until further analysis.

2.2. Methods.

2.2.1. Preparation of *Matricaria chamomilla* L. plants (chamomile flower).

The collected leaves of the chamomile flower were cleaned with distilled water to remove impurities. The leaves were then dried in an oven to eliminate all moisture. Subsequently, 40 g of the dried leaves were ground into a fine powder using a pestle and mortar. The crushed leaves were boiled in 100 mL of deionized water for approximately 2 hours at 50℃ until the water turned green and then brown, as depicted in Figure 1a. The mixture was allowed to cool to room temperature for 10-15 minutes before filtering the extract through Whatman filter paper. The aqueous extract was stored at room temperature for future use.

2.2.2. Green synthesis of zinc oxide nanoparticles.

The synthesis of zinc oxide nanoparticles (ZnONPs) was carried out using the co-precipitation method. An aqueous solution of zinc acetate (0.02 M) was prepared by adding 0.02 g of zinc acetate to 50 mL of distilled water and stirring vigorously for 15 minutes. Afterward, different ratios of plant extract (1.0 mL, 2.0 mL, 3.0 mL, and 4.0 mL) were added to the zinc acetate dehydrate solution. Next, 2.0 M of NaOH solution was added to the mixture to form a white aqueous solution, which was then stirred for 2 hours. The residue was then washed with distilled water and ethanol to remove impurities, followed by calcination in a furnace at 300 °C for 4-5 hours. The resulting product was a brownish powder, which was identified as ZnONPs.

2.2.3. Characterization of zinc oxide nanoparticles.

The synthesized ZnONPs were analyzed for structure, optical properties, and morphology using X-ray diffraction (XRD), a UV-visible spectrophotometer, Fourier transform infrared spectroscopy (FTIR), and scanning electron microscopy (SEM). XRD was used to determine the crystalline structure of the nanoparticles, and the UV-Visible Spectrophotometer was used to analyze their optical properties. The FTIR provided information on the functional groups present in the nanoparticles, and the SEM was used to examine their size and shape. After these characterizations, the prepared ZnONPs were studied for potential photovoltaic applications.

3. Results and Discussion

3.1. Optical properties.

The UV-visible spectroscopy analysis of the prepared zinc oxide nanostructure sample at room temperature in Figure 1 revealed that the sample absorbs radiation in the UV region, specifically between 200-400 nm, while the visible spectrum radiation is transmitted. The sharp absorption peak at around 361.75 nm is an indication of the excitonic characteristics of the zinc oxide nanostructure at room temperature. This result highlights the potential of the prepared zinc oxide nanostructure in enhancing light absorption and carrier generation in solar cells.

The bandgap energy of the ZnO nanoparticles was calculated by extrapolating the curve between the frequency (ν) and the optical absorption coefficient (α) using equations 1 to 3, as revealed in Figure 2. The resulting band gap energy was approximately 3.3 eV, confirming the semiconducting nature of the ZnO nanoparticles and their suitability for photovoltaic

applications. These findings suggest that the ZnO nanoparticles have the potential to be used in solar cells for converting solar energy into electrical energy.

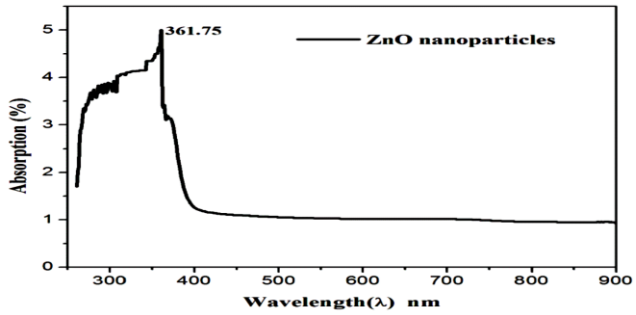

Figure 1. UV-visible absorption spectra of zinc oxide nanoparticles.

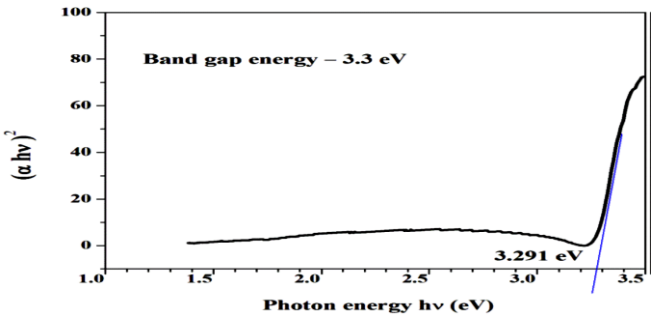

Figure 2. Extrapolation curve for the bandgap of prepared ZnO nanoparticles.

The absorption coefficient (α) and the optical band gap (E_g) of the thin film were determined by Equations 1-3 [29–31];

$$\alpha = 2.303(\frac{A}{t}) \quad (1)$$

Where A is absorbance, and t is the thickness. The absorption coefficient α and the extinction coefficient k are related by the equation

$$k = \frac{a\lambda}{4\pi} \quad (2)$$

Where λ is the wavelength.

The equation relates the optical band gap energy Eg and absorption coefficient α

$$(\alpha hv)^2 = hv - E_G \quad (3)$$

where h = Planck's constant = 6.626 x 10^{-34} Joules sec. c is the speed of light = 3.0 x 10^8 meters/sec. where 1 ev =1.6 x 10^{-19} Joules.

3.2. SEM analysis.

The SEM images in Figure 3a reveal that the particles are spherical and granular. Higher-resolution SEM imaging reveals particle agglomeration, which may be due to aging. The size distribution of the prepared Zinc Oxide nanoparticles, as shown in Figure 3b, is well fit by a Gaussian distribution, indicating a very uniform distribution throughout the solution.

3.3. XRD analysis.

The ZnO nanoparticles (ZnONPs) were analyzed using X-ray diffraction (XRD) with a D8 Advance Bruker AXS instrument. The XRD pattern in Figure 4 shows the diffraction analysis of the ZnNPs in powder form, covering angles from 10° to 90º. Notable diffraction peaks were observed at Bragg's angles of 32.37°, 35.53°, 36.12°, 47.4°, 56.2°, 62.55°, 67.3°, and 69.1°, corresponding to the crystallographic planes (100), (002), (101), (102), (110), (103),

(112), and (201) respectively. This XRD pattern provided insights into the orientation and crystalline structure of the ZnONPs. To determine the phase speciation, the obtained XRD pattern was compared with the International Center for Diffraction Data (ICDD) reference data for Zn.

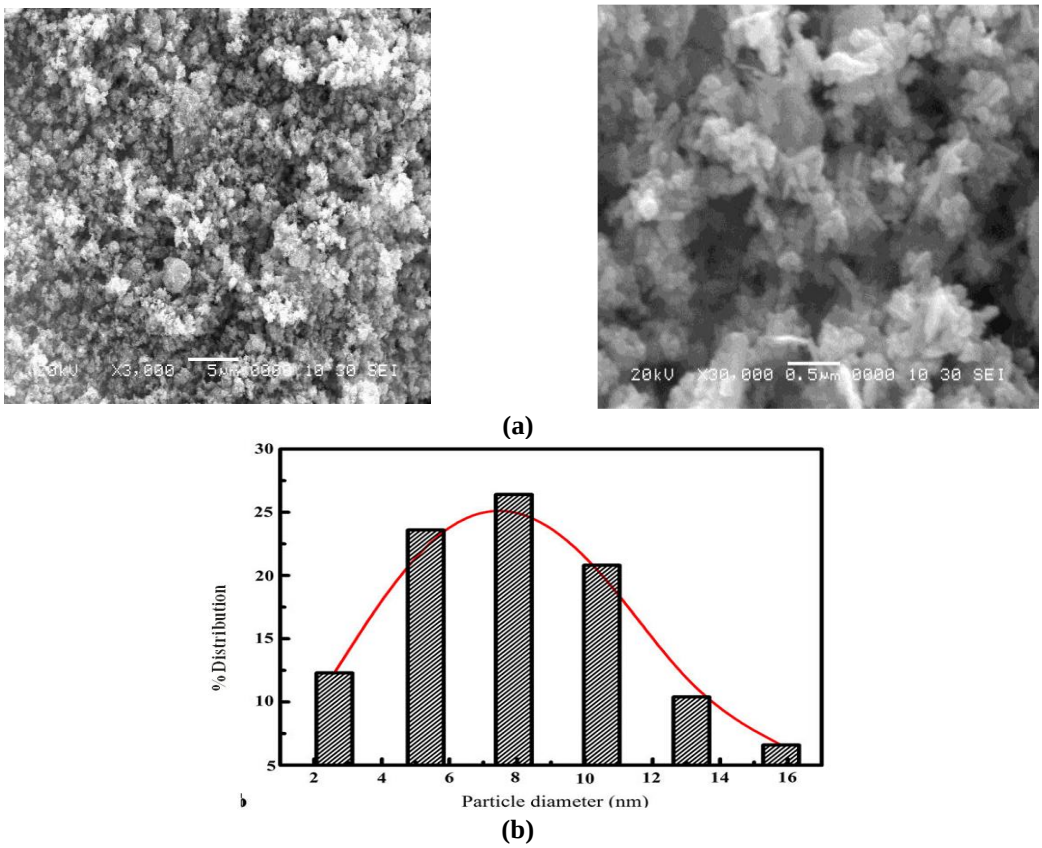

Figure 3. (a) SEM image of zinc oxide nanoparticles at different resolutions; **(b)** The calculated size distribution of green-synthesized zinc oxide nanoparticles with a Gaussian fit.

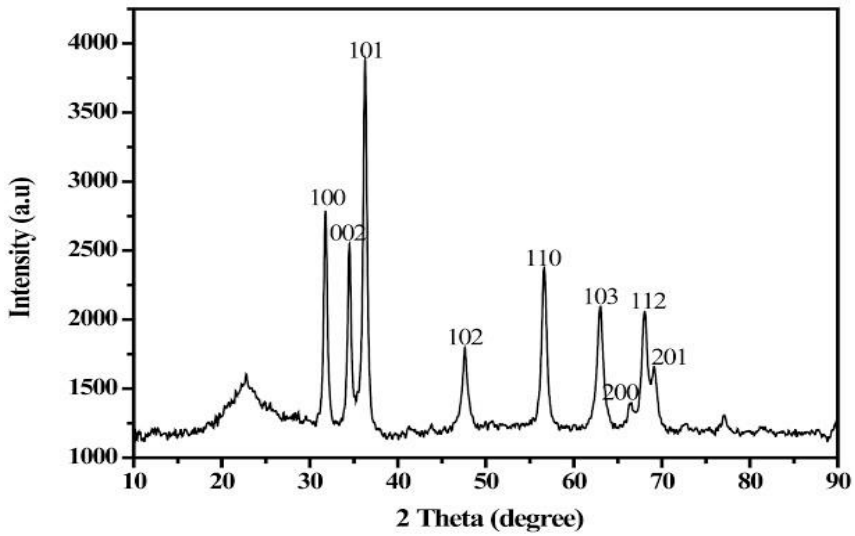

Figure 4. XRD patterns of zinc oxide nanoparticles.

This comparison confirmed the successful synthesis of ZnONPs through the green synthesis method, resulting in the formation of crystalline wurtzite hexagonal structures. The crystallite size (D) of the ZnONPs was calculated using the Scherrer equation from the (101) peak in the XRD graph, providing valuable information on the average crystallite size of the synthesized ZnONPs. These results are consistent with recent research by {Formatting

Citation}, who reported the synthesis of hexagonal wurtzite ZnO nanoparticles via a hydrothermal method.

$$D = \frac{0.9\lambda}{\beta cos\theta} \quad (4)$$

where λ is the x-ray wavelength, θ = the Bragg diffraction angle, and β = the FWHM of the peak appearing at the diffraction angle. The calculated average size of the ZnONP was found to be approximately 36 nm. This value is consistent with the expected size range for nanoparticles and indicates the successful synthesis of ZnONP with a narrow size distribution.

3.4. Effect of spin-coater speed (rpm) on the thickness of ZnONP-based polymer solar cells.

The investigation focused on the effect of spin-coater revolutions per minute (rpm) on the thickness of the ZnO film deposited on a glass substrate. By examining the ZnO nanoparticles buffer layer created at various rotation speeds, we analyzed the absorption peaks as depicted in Figure 5. It was observed that an optimal rpm of 1500 best enhances conditions for improved photovoltaic performance.

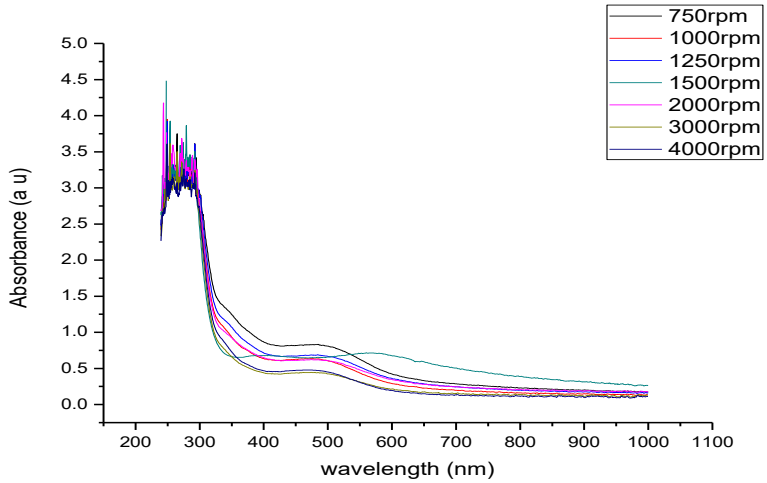

Figure 5. Absorbance of ZnO nanoparticle thin films at different rpm.

The effect of varying thermal annealing temperature on the UV-Vis characteristics of Zinc Oxide nanoparticle-based buffer layer films was investigated across a temperature range of 50℃ to 300℃ (Figures 6-9). The study revealed that an annealing temperature of 300℃ yielded optimal conditions for achieving maximum absorbance, transmittance, and reflectance in the films, as depicted in Figures 7-9. This temperature setting is crucial for maximizing device performance by ensuring superior optical properties and electron-transfer efficiency within the thin-film structure.

The study found that thermal annealing enhances the quality of film deposition and the crystallinity of ZnO nanoparticles in the buffer layer, which, in turn, improves the efficiency of the solar cell by increasing the transmission of photo-generated electrons to the anode. This is achieved by optimizing the optical properties of the film, including its absorbance, transmittance, and reflectance. The optimal annealing temperature for achieving the best maximum absorbance, transmittance, and reflectance was found to be 300℃, which is in close agreement with a previous study that the surface morphology of ZnO nanostructures deposited on a quartz substrate was highly uniform when the optimum preparation conditions (400℃) [33]. This temperature setting is crucial for maximizing the performance of the device by

ensuring superior optical properties and electron transfer efficiency within the thin film structure.

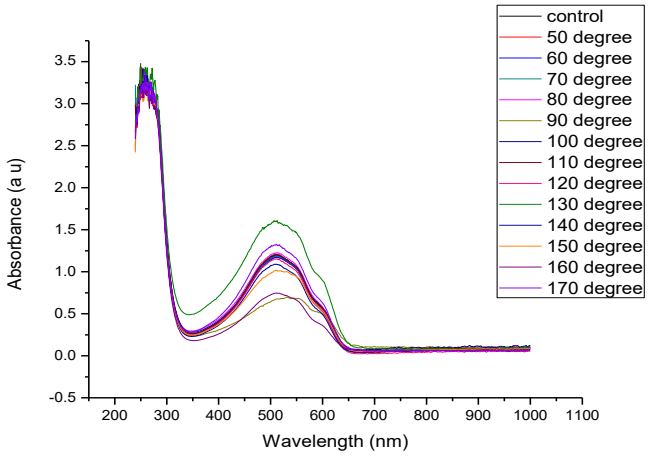

Figure 6. Post-thermal annealing on the absorbance spectra.

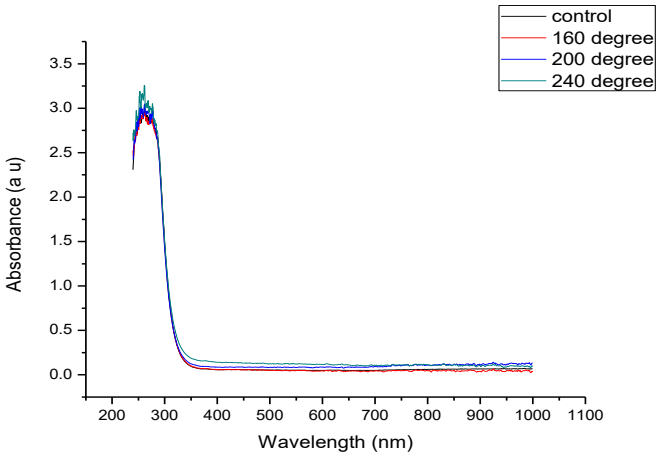

Figure 7. Effect of thermal annealing on absorbance spectra.

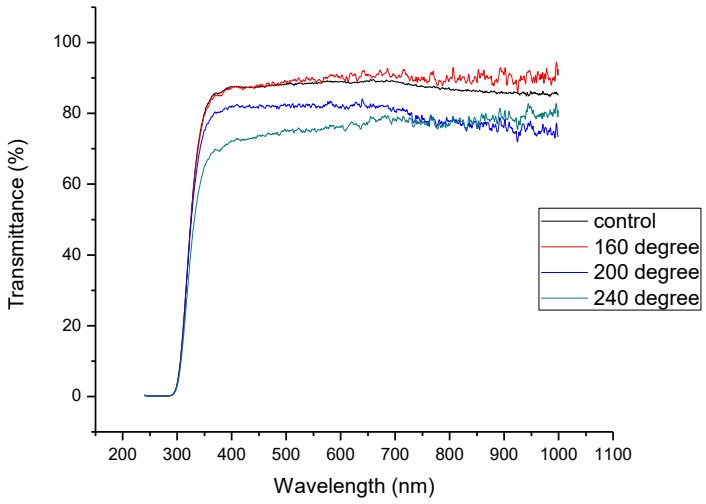

Figure 8. Effect of thermal annealing on transmittance spectra.

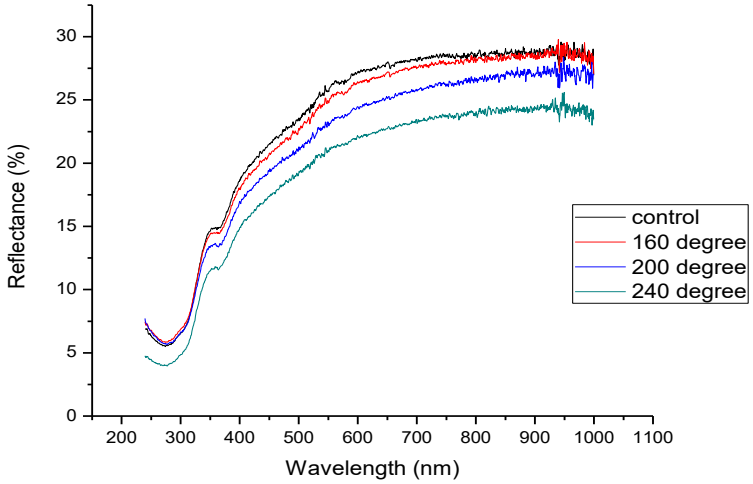

Figure 9. Effect of thermal annealing on reflectance spectra.

3.4. The optimization of processing parameters for enhancing the electrical properties of zinc oxide buffer layer thin-film devices.

The ZnO film was subjected to annealing at varying temperatures and durations to optimize the processing parameters. The performance of the ZnO nanoparticles buffer layer device under different processing conditions is presented in Table 1. It has been established that the optimal spin-coating speed for achieving the best performance was 1500 rpm, and the device exhibited significant improvements across various annealing conditions and times with this speed compared to devices with other speeds.

For example, the device annealed at 300℃ for 1 hour exhibited a current (I) of 9.48 mA/cm^2, voltage (V) of 0.45V, maximum power of 4.266, resistance of 2.93 Ω/cm^2, and sheet resistance of 296.7 Ω/cm^2. Similarly, the device annealed at 400 ℃ for 10 minutes displayed a current (I) of 9.40 mA/cm^2, voltage (V) of 0.44V, maximum power of 3.324, resistance of 2.76 Ω/cm^2, and sheet resistance of 294.4 Ω/cm^2. Furthermore, the device annealed at 300℃ for 30 minutes showed a current (I) of 9.50 mA/cm^2, voltage (V) of 0.46V, maximum power of 4.37, resistance of 2.16 Ω/cm^2, and sheet resistance of 291.8 Ω/cm^2, indicating remarkable improvements in the thin film organic solar cells.

Table 1. Performance characteristics of ZnO buffer layer thin film with different spin-coating speeds, annealing time, and annealing temperatures.

Speed of zinc (rpm)	Annealing condition	Time (sec)	V (v)	I (mA/cm^2)	Power (w)	R (Ω/cm^2)	R_{sh} (Ω/cm^2)
1500	100℃	1hr	0.50	9.23	3.79	3.97	436
1500	100℃	45 min	0.52	9.45	3.96	4.23	422
1500	100℃	30 min	0.51	9.40	3.82	3.36	431
1500	200℃	1hrs	0.53	8.99	3.86	4.81	301
1500	200℃	45 min	0.52	8.98	3.86	4.45	313
1500	200℃	30 min	0.52	9.01	3.72	4.61	347
1500	300℃	1hr	0.65	9.48	4.36	2.95	346
1500	300℃	45 min	0.63	9.50	4.37	2.26	293
1500	300℃	30 min	0.60	9.40	3.35	2.70	296

3.5. Photovoltaic performance.

The typical I-V characteristics of devices incorporating green-synthesized zinc oxide nanoparticles are depicted in Figure 10. The average short-circuit current density (Jsc), open-circuit voltage (Voc), fill factor (FF), and power conversion efficiency (PCE) values for each device are presented for comparison purposes. It is noteworthy that the buffer layer device

utilizing chemically prepared zinc oxide exhibits a Jsc of 0.690 mA/cm^2, a Voc of 0.580 V, and FF of 0.812, yielding a PCE of 3.580 %. This lower performance can be attributed to the high leakage current resulting from the low work function of the buffer layer device with chemically prepared zinc oxide. In contrast, the device employing green synthesized zinc oxide demonstrates a Jsc of 0.750 mA/cm, a Voc of 0.740 V, and FF of 0.895, resulting in a PCE of 4.320 %. These results indicate that the green-synthesized zinc oxide film can serve as an effective substitute for the buffer layer, leading to improved device performance and, consequently, enhanced overall performance of organic solar cells.

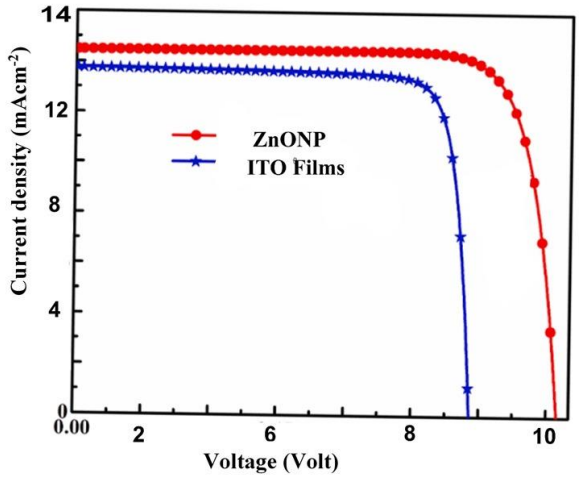

Figure 10. Current – Voltage (I–V) characteristic curve of nanoparticle-based polymer solar cell.

Table 2. I–V characteristics parameters of nanoparticle-based polymer solar cell.

Thin film devices	*Isc* (mA/cm^2)	*Voc* (V)	Fill factor	PCE (%)
ITO film	0.690	0.580	0.812	3.580
Green ZnONP	0.790	0.740	0.895	4.320

4. Conclusions

In this study, ZnONP has been successfully synthesized using the spin coating method. Examination under SEM revealed the prepared film to be homogeneous. It was also revealed that thermal annealing improved the quality of the deposited film. Optical analyses reveal a promising prospect for the applications of ZnONPs in photovoltaic systems.

Author Contributions

Conceptualization, A.A.A. and Y.K.S.; methodology, S.O.A.; validation, K.O.S. and A.A.A.; formal analysis, K.O.S.; investigation, K.O.S. and S.O.A.; resources, A.A.O.; data curation, K.K.B.; writing—original draft preparation, S.O.A.; writing—review and editing, K.O.S. and A.A.O.; supervision, Y.K.S.; project administration, A.A.A. All authors have read and agreed to the published version of the manuscript.

Institutional Review Board Statement

Not applicable.

Informed Consent Statement

Not applicable.

Data Availability Statement

Data supporting the findings of this study are available upon reasonable request from the corresponding author.

Funding

This research received no external funding.

Acknowledgments

The authors would also like to appreciate the Material Science Research Laboratory, Kwara State University, Malete, Nigeria, for making their facilities available for the material characterization.

Conflicts of Interest

The authors declare no conflict of interest.

References

1. Li, X.; Lepour, D.; Heymann, F.; Maréchal, F. Electrification and digitalization effects on sectoral energy demand and consumption: A prospective study towards 2050. *Energy* **2023**, *279*, 127992, https://doi.org/10.1016/j.energy.2023.127992.
2. Burke, P.J.; Stern, D. .; Bruns, S.B. The Impact of Electricity on Economic Development: A Macroeconomic Perspective. *Int. Rev. Environ. Resour. Econ.* **2018**, *12*, 85-127, https://doi.org/10.1561/101.00000101.
3. Gkalonaki, S.; Karatzas, K. Assessing the environmental impacts of renewable energy sources with emphasis on wind energy. *IOP Conf. Ser.: Earth Environ. Sci.* **2022**, *1123*, 012053, https://doi.org/10.1088/1755-1315/1123/1/012053.
4. Chen, X.H.; Tee, K.; Elnahass, M.; Ahmed, R. Assessing the environmental impacts of renewable energy sources: A case study on air pollution and carbon emissions in China. *J. Environ. Manag*. **2023**, *345*, 118525, https://doi.org/10.1016/j.jenvman.2023.118525.
5. Majeed, Y.; Khan, M.U.; Waseem, M.; Zahid, U.; Mahmood, F.; Majeed, F.; Sultan, M.; Raza, A. Renewable energy as an alternative source for energy management in agriculture. *Energy Rep.* **2023**, *10*, 344-359, https://doi.org/10.1016/j.egyr.2023.06.032.
6. Kantoğlu, B.; Argun, İ.D. Evaulation of renewable energy source alternatives prioritization. *Turkish J. Eng.* **2023**, *7*, 1-8, https://doi.org/10.31127/tuje.1001488.
7. Centi, G.; Iaquaniello, G.; Perathoner, S. Chemical engineering role in the use of renewable energy and alternative carbon sources in chemical production. *BMC Chem. Eng.* **2019**, *1*, 5, https://doi.org/10.1186/s42480-019-0006-8.
8. Jolivet, A.; Cardin, J.; Cheik, A.; Frilay, C.; Gourbilleau, F.; Lemarié, F.; Portier, X.; Jadwisienczak, W.; Ingram, D.; Mezhoud, M.; Lüders, U.; Fouchet, A.; Labbé, C. Strontium Vanadate Deposited by ALD: Toward a New Synthesis Approach. *ECS Meet. Abstr.* **2023**, *MA2023-02*, 1489, https://doi.org/10.1149/ma2023-02291489mtgabs.
9. Shankar, U.; Oberoi, D.; Bandyopadhyay, A. A review on the alternative of indium tin oxide coated glass substrate in flexible and bendable organic optoelectronic device. *Polym. Adv. Technol.* **2022**, *33*, 3078-3111, https://doi.org/10.1002/pat.5797.
10. Ramarajan, R.; Joseph, D.P.; Thangaraju, K.; Kovendhan, M. 13 - Role of defects on the transparent conducting properties of binary metal oxide thin film electrodes. In Metal Oxide Defects, Kumar, V., Som, S., Sharma, V., Swart, H.C., Eds.; Elsevier: **2023**; pp. 387-420, https://doi.org/10.1016/B978-0-323-85588-4.00003-9.
11. Wang, B.; Huang, W.; Bedzyk, M.J.; Dravid, V.P.; Hu, Y.-Y.; Marks, T.J.; Facchetti, A. Combustion Synthesis and Polymer Doping of Metal Oxides for High-Performance Electronic Circuitry. *Acc. Chem. Res.* **2022**, *55*, 429-441, https://doi.org/10.1021/acs.accounts.1c00671.

12. Rahman, S.; Haleem, A.; Siddiq, M.; Hussain, M.K.; Qamar, S.; Hameed, S.; Waris, M. Research on dye sensitized solar cells: recent advancement toward the various constituents of dye sensitized solar cells for efficiency enhancement and future prospects. *RSC Adv.* **2023**, *13*, 19508-19529, https://doi.org/10.1039/d3ra00903c.
13. Sverdrup, H.U.; van Allen, O.; Haraldsson, H.V. Modeling Indium Extraction, Supply, Price, Use and Recycling 1930–2200 Using the WORLD7 Model: Implication for the Imaginaries of Sustainable Europe 2050. *Nat. Resour. Res.* **2024**, *33*, 539-570, https://doi.org/10.1007/s11053-023-10296-z.
14. Jeong, Y.; Pearson, C.; Lee, Y.U.; Ahn, K.; Cho, C.-R.; Hwang, J.; Kim, H.; Do, L.-M.; Petty, M.C. Effects of hydrogen plasma treatment on the electrical behavior of solution-processed ZnO transistors. *J. Appl. Phys.* **2014**, *116*, 074509, https://doi.org/10.1063/1.4893470.
15. Abd El-Latif, S.T.; Ahmed, K.M.; Elkalashy, S.I.; Zaki, M.F. Atmospheric–pressure DBD plasma modifying photoemission, optical and electrical properties of polycarbonate films. *Inorg. Chem. Commun.* **2024**, *161*, 112048, https://doi.org/10.1016/j.inoche.2024.112048.
16. Huang, T.; Mo, C.; Cui, M.; Li, M.; Ji, P.; Tan, H.; Zhang, X.; Zhuge, L.; Wu, X. Ion behavior impact on ITO thin film fabrication via DC magnetron sputtering with external anode. *Vacuum* **2024**, *221*, 112848, https://doi.org/10.1016/j.vacuum.2023.112848.
17. Kumar, V.; Prakash, J.; Pathak, D.; Sharma, D.P.; Purohit, L.P.; Swart, H.C. Ion beam engineering of implanted ZnO thin films for solar cell and lighting applications. *Chem. Eng. J. Adv.* **2023**, *15*, 100501, https://doi.org/10.1016/j.ceja.2023.100501.
18. Loh, L.; Dunn, S. Recent Progress in ZnO-Based Nanostructured Ceramics in Solar Cell Applications. *J. Nanosci. Nanotechnol* **2012**, *12*, 8215–8230, https://doi.org/10.1166/jnn.2012.6680.
19. Shiyani, T.; Mahapatra, S.K.; Banerjee, I. Natural Basil as Photosensitizer with ZnO Thin Films for Solar Cell Applications. *IETE J. Res.* **2022**, *68*, 3439-3446, https://doi.org/10.1080/03772063.2020.1768161.
20. Otalora, C.; Botero, M.A.; Ordoñez, G. ZnO compact layers used in third-generation photovoltaic devices: a review. *J. Mater. Sci.* **2021**, *56*, 15538–15571, https://doi.org/10.1007/s10853-021-06275-5.
21. Badawi, A.; Althobaiti, M.G.; Ali, E.E.; Alharthi, S.S.; Alharbi, A.N. A comparative study of the structural and optical properties of transition metals (M = Fe, Co, Mn, Ni) doped ZnO films deposited by spray-pyrolysis technique for optoelectronic applications. *Opt. Mater.* **2022**, *124*, 112055, https://doi.org/10.1016/j.optmat.2022.112055.
22. Nayak, S.; Kumar, P. Review on structure, optical and magnetic properties of cobalt doped ZnO nanoparticles. *Mater. Today Proc.* **2023**, https://doi.org/10.1016/j.matpr.2023.01.318.
23. Manjeet; Kumar, A.; Anu; Lohan, R.; Deopa, N.; Kumar, A.; Chahal, R.P.; Dahiya, S.; Punia, R.; Rao, A.S. Impact of Sm^{3+} ions on structural, thermal, optical and photoluminescence properties of ZnO–Na_2O–PbO–B_2O_3 glasses for optoelectronics device applications. *Opt. Mater.* **2023**, *139*, 113778, https://doi.org/10.1016/j.optmat.2023.113778.
24. Shetti, N.P.; Bukkitgar, S.D.; Reddy, K.R.; Reddy, C.V.; Aminabhavi, T.M. ZnO-based nanostructured electrodes for electrochemical sensors and biosensors in biomedical applications. *Biosens. Bioelectron.* **2019**, *141*, 111417, https://doi.org/10.1016/j.bios.2019.111417.
25. Sha, R.; Basak, A.; Maity, P.C.; Badhulika, S. ZnO nano-structured based devices for chemical and optical sensing applications. *Sens. Actuators Rep.* **2022**, *4*, 100098, https://doi.org/10.1016/j.snr.2022.100098.
26. Jia, J.; Zhu, H.; Liu, W.; Li, B.; Shi, Z.; Cui, Q.; Xu, C. Temperature Sensors Based on Negative Temperature Coefficient of ZnO Thin Films. *IEEE Trans. Electron Devices* **2023**, *70*, 5856-5862, https://doi.org/10.1109/TED.2023.3314400.
27. Mariselvam, K.; Arun Kumar, R.; Rajeswara Rao, V. Concentration-dependence and luminescence studies of erbium doped barium lithium fluoroborate glasses. *Opt. Laser Technol.* **2019**, *118*, 37-43, https://doi.org/10.1016/j.optlastec.2019.04.028.
28. Chouikh, F.; Beggah, Y.; Ariche, N.; Biréme, M.; Leroy, G.; Waldhoff, N.; Aida, M.S. A Comparative Study of Al and Bi Addition in the Transparent Conductive ZnO Thin Films Prepared by Spray Ultrasonic Method. *Int. J. Thin. Fil. Sci. Tec* **2019**, *8*, 101-112.
29. Al-Saadi, T.M.; Hussein, B.H.; Hasan, A.B.; Shehab, A.A. Study the Structural and Optical Properties of Cr doped SnO_2 Nanoparticles Synthesized by Sol-Gel Method. *Energy Procedia* **2019**, *157*, 457-465, https://doi.org/10.1016/j.egypro.2018.11.210.
30. Themlin, J.M.; Sporken, R.; Darville, J.; Caudano, R.; Gilles, J.M. Resonant-photoemission study of SnO_2: Cationic origin of the defect band-gap states. *Phys. Rev. B* **1990**, *42*, 11914, https://doi.org/10.1103/physrevb.42.11914.

31. Omar, M.A. Elementary Solid State Physics: Principles and Applications. 2nd edition; Addison Wesley Publishing Company: **1993**; pp. 176-252.
32. Khudiar, S.S.; Mutlak, F.A.H.; Nayef, U.M. Synthesis of ZnO nanostructures by hydrothermal method deposited on porous silicon for photo-conversion application. *Optik* **2021**, *247*, 167903, https://doi.org/10.1016/j.ijleo.2021.167903.
33. Badr, B.A.; Mohammed, Q.Q.; Numan, N.H.; Fakhri, M.A.; Abdul Wahhab, A.W. Substrate Temperature Effects on Optical Properties and Constants of ZnO. *Int. J. Nanoelectron. Mater.* **2019**, *12*, 283-290.

Publisher's Note & Disclaimer